Micro-milling process improvement using an agile pulse-shaping fiber laser

David Gay, Alain Cournoyer, Pascal Deladurantaye, Martin Briand, Vincent Roy, Bruno Labranche, Marc Levesque and Yves Taillon

INO, 2740 Einstein Street, Quebec City, QC, G1P 4S4

ABSTRACT

We demonstrate the usefulness of INO's pulse-shaping fiber laser platform to rapidly develop complex laser micro-machining processes. The versatility of such laser sources allows for straightforward control of the emitting energy envelop on the nanosecond timescale to create multi-amplitude level pulses and/or multi-pulse regimes. The pulses are amplified in an amplifier chain in a MOPA configuration that delivers output energy per pulse up to 60 μJ at 1064 nm at a repetition rate of 200 kHz with excellent beam quality ($M^2 < 1.1$) and narrow line widths suitable for efficient frequency conversion. Also, their pulse-on-demand and pulse-to-pulse shape selection capability at high repetition rates makes those agile laser sources suitable for the implementation of high-throughput complex laser processing. Micro-milling experiments were carried out on two metals, aluminum and stainless steel, having very different thermal properties. For aluminum, our results show that the material removal efficiency depends strongly on the pulse shape, especially near the ablation threshold, and can be maximized to develop efficient laser micro-milling processes. But, the material removal efficiency is not always correlated with a good surface quality. However, the roughness of the milled surface can be improved by removing a few layers of material using another type of pulse shape. The agility of INO's fiber laser enables the implementation of a fast laser process including two steps employing different pulse characteristics for maximizing the material removal rate and obtaining a good surface quality at the same time. A comparison of material removal efficiency with stainless steel, well known to be difficult to mill on the micron scale, is also presented.

Keywords: Pulsed fiber laser, MOPA, pulse shaping, laser material processing, micro-milling, surface roughness.

1. INTRODUCTION

Flexible pulsed fiber laser sources having a MOPA configuration are emerging as alternatives to traditional DPSS Q-switched lasers for developing advanced laser processes in various technical fields. The possibility of controlling the pulse characteristics (rise time, width, temporal shape, and repetition rate) with a great precision and in a straightforward manner allows for exploring new laser processing capabilities using a single laser source. MOPA pulsed fiber sources can be designed to operate at high repetition rates with narrow line widths and excellent beam quality, making them suitable sources for applications like memory repair, solar cell micromachining and micro-milling in metals. In this paper we present micro-milling results obtained with stainless steel and aluminum, using one version of the INO industrial pulsed fiber MOPA laser platform offering programmable pulse shapes at the nanosecond time scale.

In industrial laser milling, the material removal rate, which depends on scan speed, laser pulse energy and/or power, and pulse repetition rate, directly determines the laser process throughput and the production rate, but also the quality of the laser-machined surfaces.[1] Sharp edges, smooth surfaces, minimum heat affected zone (HAZ), minimum recast and splatter are desirable characteristics. Hence, one can take advantage of the high repetition rates of fiber lasers to improve the laser milling process throughput, given that the adequate scan speed and/or an adequate machining routine are used to optimize the overlapping between consecutive pulses and to minimize the thermal loading of the substrate.

Picosecond and femtosecond lasers are known to exhibit the potential advantage of reducing the HAZ and improving the quality of laser-milled surfaces. However, the small amount of material removed per ultrashort pulse (when compared to a nanosecond pulse of the same energy) [2] limits the production rate of laser micro-milling. Moreover, the high repetition rates of fiber lasers give rise to thermal loading effects even in the case of ultrashort pulses,[3] which thus partly lose their advantage with respect to the quality of the laser-milled surfaces. On the other hand, nanosecond laser pulses can be temporally managed in such a way to produce "femtosecond-class" machining results.[2] Taking into

account the higher material removal rate achievable using nanosecond pulses, optimization of the temporal shape of the pulses is an interesting way to improve both the throughput and the quality of the laser micro-milling process.

The main objective of the experiments carried out in this work was to demonstrate how a flexible MOPA fiber laser source can be advantageously exploited for optimizing laser micro-milling in metals. First, the influence of both the nanosecond-scale laser pulse energy and the pulse duration on material removal efficiency (measured in $\mu m^3/\mu J$), and the laser-milled surface roughness were studied. Then, for a given pulse duration, we studied the influence of the pulse temporal shape on the material removal efficiency and the surface roughness. Although our fiber laser technology allows for it in principle, we did not attempt, at this stage, to find the optimum laser pulse parameters. For example, we did not investigate the double-pulse scheme (which can be reproduced with even more flexibility using our MOPA fiber laser technology) developed at General Atomics and used by Forsman *et al.*[2] to achieve "femtosecond-class" drilling results in metals. We nevertheless showed how our flexible fiber laser technology could improve laser micro-milling efficiency and laser-milled surface quality using *in-process* temporal pulse shaping capabilities.

2. EXPERIMENTAL SETUP AND METHODOLOGY

2.1 MOPA laser system

Two different master oscillators (MO) developed at INO and offering pulse shaping agility were considered for the different micro-machining experiments. Both lasers used the same embedded digital industrial laser pulse shaping platform allowing for programming pulse shapes easily from a remote computer communicating with the laser. In this platform, called MOPAW (***M**aster **O**scillator with **P**rogrammable **A**rbitrary **W**aveform*), a digital control unit (DCU) and a high-speed digital-to-analog converter (DAC) are used in conjunction to generate a pulse having a predetermined amplitude profile or shape. The DCU generates a waveform by concatenation of consecutive temporal "bins", the amplitude of each "bin" being programmed independently with a 10-bit resolution. Each "bin" has a temporal width of 2.5 ns and 1 to 32 "bins" can be addressed, thus allowing pulse durations in the range of 2.5 ns to 80 ns. Up to 32 different pulse shapes can be stored in memory and pulse-to-pulse shape selection at high repetition rates (up to 1 MHz) is available for processes asking for pulse shaping on demand. The difference between the two master oscillators lies in their optical architectures using two different optical pulse generation schemes. One of the MO is based on a directly modulated laser diode whereas the other uses integrated $LiNbO_3$ electro-optic Mach-Zehnder modulators to generate the optical pulses. Both architectures are diagrammatically represented in Fig. 1. A detailed description of the modulator-based MO can be found in references [4] and [5]. Also, a new version and examples of complex pulse shapes of our MOPAW platform are found in reference [6].

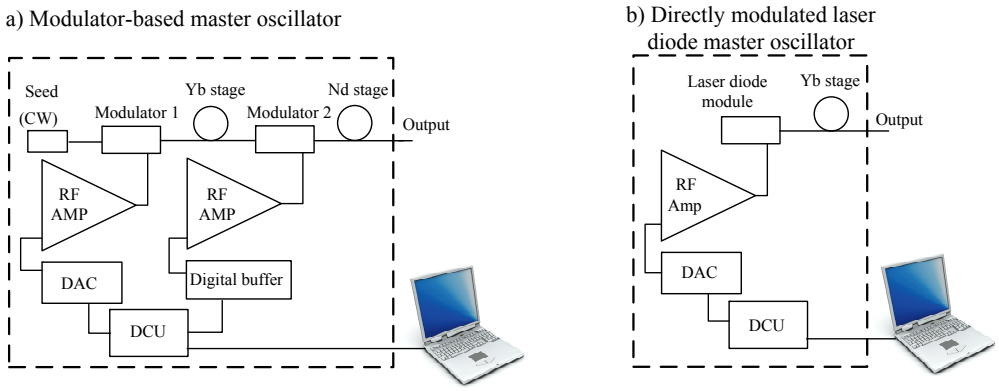

Fig. 1. Schematic representation of the two different MO architectures.

The power amplifier part of the MOPA laser system is depicted in Fig. 2. It includes an Yb-doped, polarization maintaining, cladding-pumped large-mode area (LMA) fiber as the gain medium. This fiber was designed and fabricated in our facilities, based on INO's proprietary triple clad fiber technology.[7,8] Its special core design allowed for efficiently amplifying high peak power pulses (> 1 kW) while maintaining an excellent beam quality. The large mode field diameter (16 µm) also allowed for keeping control over fiber nonlinearities such as stimulated Brillouin scattering (SBS), four-wave mixing (FWM), self-phase modulation (SPM) and stimulated Raman scattering (SRS). The most

interesting aspect of this LMA fiber is its ability to maintain stable beam characteristics under temperature changes or under thermo-mechanically induced stresses, making it a suitable device for an industrial environment.

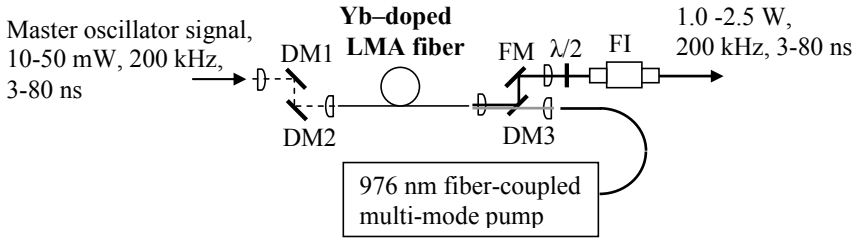

Fig. 2. Schematic view of the power amplifier of the MOPA laser system (DMx: dichroic mirrors, FM: folding mirror, FI: Faraday isolator).

In terms of pulsed optical output characteristics, the pulses generated with the directly modulated laser diode MO had a slower rise time and a broader line width compared to the modulator-based MO. However, with the former it was possible to reach higher pulse energy levels (at the expense of some amount of SPM-induced spectral broadening) at the output of the power amplifier because SBS was not a limiting factor above 10 μJ as it was the case for the other MO, which employed a narrow linewidth seed laser diode operated in the CW regime. The main advantage of the modulator-based MO in the experiments of micro-milling is the shorter rise time of the optical pulses producing sharper pulse shapes in the time domain, as one of the objectives of this work was to verify the importance of this parameter on the process quality and efficiency. Although both systems were used during our study, only the results obtained with the modulator-based MO are presented in this paper. Table 1 compares the characteristics of the laser system output for both master oscillators once amplified by the power amplifier.

Table 1. Comparison of the optical output characteristics of the MOPA laser system for the two master oscillators.

Parameter	Modulator-based MOPA	Directly modulated laser diode MOPA
Wavelength of emission	1064 nm	
Spectral linewidth	< 0.05 nm	< 0.5 nm
Pulse repetition rate	100 kHz-1 MHz, adjustable or ext. trig.	
Pulse width	3-30 ns, adjustable	3-80 ns, adjustable
Pulse shaping resolution	2.5 ns (time domain), 1024 levels (amplitude)	
Pulse rise time	1 ns	3 ns
Maximum pulse energy	10 μJ	60 μJ
Pulse-to-pulse energy stability	± 1% (10^4 pulses, 3σ)	± 1.4% (10^4 pulses, 3σ)
Pulse-to-pulse amplitude stability	± 3% (10^4 pulses, 3σ)	± 3% (10^4 pulses, 3σ)
M^2	1.05	
Beam waist astigmatism	< 10%	
Beam roundness	> 92%	
Beam waist asymmetry	< 8%	
Polarization Extinction Ratio	> 300:1, linear polarization (> 24 dB)	

2.2 Micro-milling setup and methodology

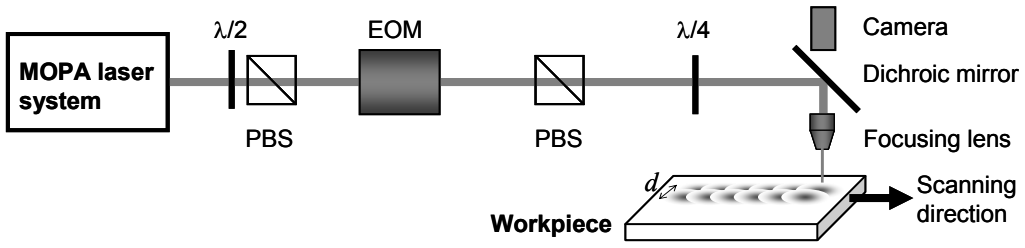

Fig. 3. Experimental setup (PBS: polarizing beamsplitters, EOM: electro-optic modulator)

The focusing lens, as shown in Fig. 3, has a focal length of 38 mm and was chosen long enough to produce a laser spot size almost constant along the total trench depth but small enough to get the necessary power densities for vaporization of the material. The trenches were made by milling several layers in a raster scan fashion. The number of grooves was set to obtain 60-µm wide trenches. No post-processing of the samples other than a simple cleaning with alcohol was done after the laser micro-milling.

Before we study the influence of pulse characteristics (energy, shape, duration) on the efficiency of laser micro-milling, the parameters related to the scanning process were first optimized. The pulse-to-pulse overlap C_{p-p} representing the degree of overlapping between the pulses along the scanning direction and the lateral overlap C_l representing the degree of overlapping between the grooves are respectively defined as

$$C_{p-p} = \left(1 - {s_s}/{f_p \phi}\right) \qquad \text{and} \qquad C_l = \left(1 - {d}/{\phi}\right) \tag{1}$$

where s_s is the scanning speed, f_p the repetition rate, ϕ the laser spot diameter, and d is the distance between two consecutive grooves. By using 10-ns square-shaped pulses and an 11-µm laser spot diameter, we found that the optimum values for C_{p-p} and C_l are around 57% and 48%, respectively, as shown on Figs 4 and 5. Further reduction of the lateral overlap results in such deterioration in the quality of surface that trench depth becomes very difficult to assess. The optimization of both overlaps was based on the capacity for a laser pulse (of energy E_p) to remove a certain volume of material (V_p), defined as the material removal efficiency. This can be calculated using the following equation:

$$Efficiency = \frac{V_p}{E_p} = \frac{\Delta z_n \cdot s_s \cdot d}{E_p \cdot f_p \cdot n} \quad \left[\mu m^3/\mu J\right], \tag{2}$$

where Δz_n is the total trench depth and n is the number of ablated layers. Because of the speed limitation of our high-precision positioning system to match the high repetition rate of the laser, the optimum pulse-to-pulse overlap was obtained by reducing the repetition rate of the pulse train (down to 400 Hz) using an electro-optic modulator combined with a polarizing beamsplitter. Indeed, a very poor surface quality during laser milling tests on stainless steel was observed at a full scanning speed and with a pulse train at maximum f_p, leading to a high C_{p-p} of 98.3 %. In the case of laser milling on steel and aluminum alloys, an optimized C_{p-p} around 50% or less for minimum surface roughness has also been reported[9,10] by other authors even though their process involved repetition rates in the tens of kilohertz.

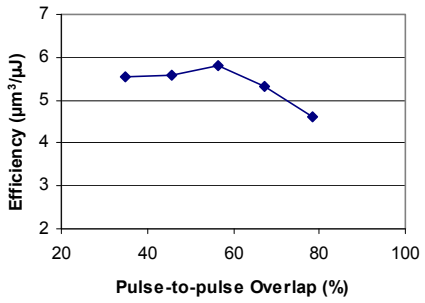

Fig. 4. Material removal efficiency as a function of the pulse-to-pulse overlap in aluminum.

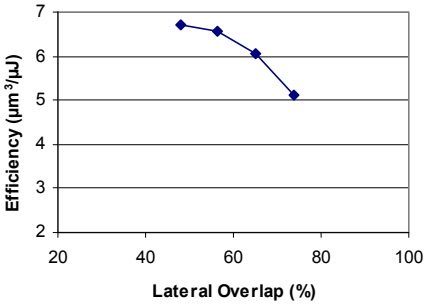

Fig. 5. Material removal efficiency as a function of the lateral overlap in aluminum.

3. EXPERIMENTAL RESULTS

In this section, we present an analysis of the material removal efficiency and the milled surface roughness as a function of the energy/pulse, the pulse duration and the pulse shape for two metals, aluminum and stainless steel. Both overlapping parameters were kept constant at their optimum values as mentioned before. The SEM images show trenches created by a sequence of ablated layers (20 in the case of aluminum and 40 to 60 in the case of stainless steel were needed to obtain high depths that can be accurately measured).

3.1 Laser micro-milling of aluminum

Fig. 6(a) illustrates, for different laser pulse energies, the effect of the duration of square-shaped pulses on the material removal efficiency ($\mu m^3/\mu J$) of aluminum. Indirectly, the influence of laser pulse peak power density (MW/cm^2) can be also inferred, since it proportionally decreases as the pulse duration increases for a given energy. The results can be understood on a phenomenological basis with the presence of plasma effects that prevent material removal, such as laser incident energy absorption and scattering in the plasma (shielding effect) [11]. As the power density decreases with increasing pulse duration for a given pulse energy, more of the laser pulse energy is absorbed at the surface of the aluminum substrate until an optimum value is reached. The optimum value of the power density is approximately 180-190 MW/cm^2, which is in the range of typical values for plasma ignition in the nanosecond regime [11], and is constant over the energy range used (as indicated in Fig. 6(a)). For pulse durations longer than the optimum value, the efficiency decreases as the power density approaches the threshold for vaporization, located near 90 MW/cm^2 (from the results of Fig. 6(a)). The efficiencies obtained with sloped-top square-shaped pulses (815-ps rise time) are slightly better when compared to flat-top square-shaped pulses (1.5-ns rise time). Nevertheless, it was not possible to identify which of the rise time or the slightly different shape was the main factor in explaining the efficiency improvement.

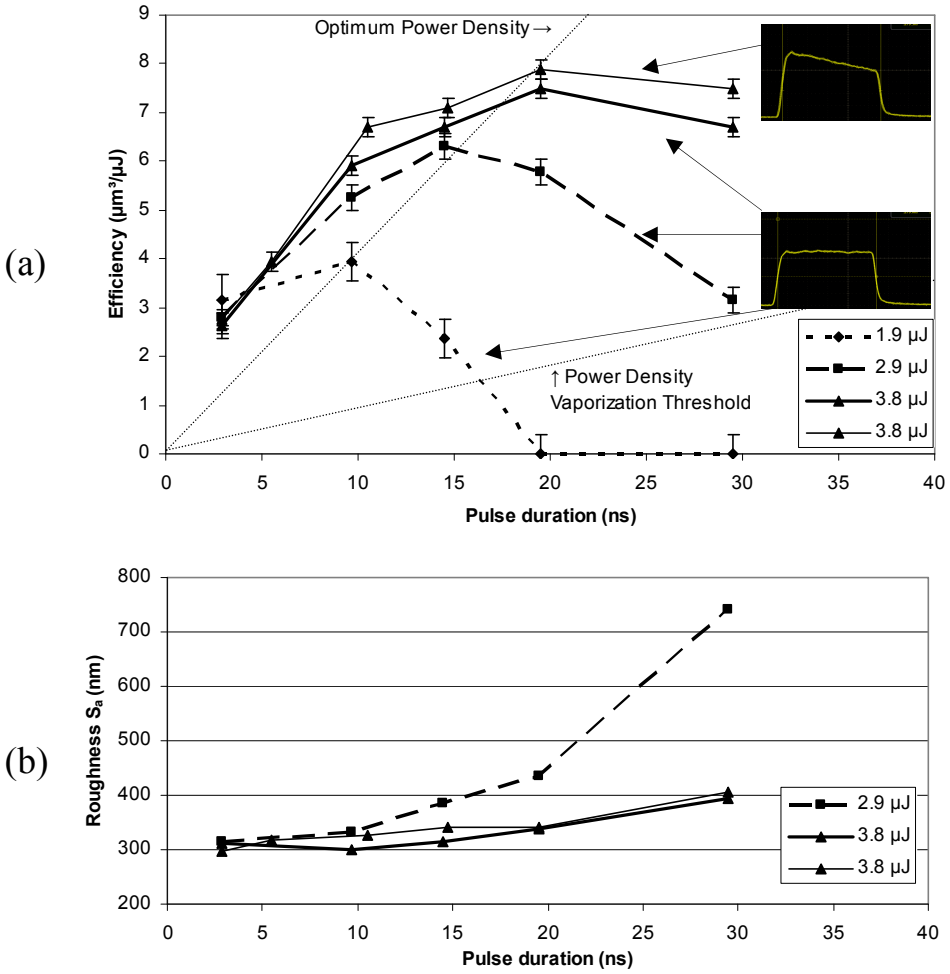

Fig. 6. (a) Material removal efficiency and (b) average roughness in aluminum as a function of pulse duration of a square-shaped pulse. Flat-top and sloped-top pulses are represented by thick and thin lines, respectively. Each dotted guideline intersect efficiency curves at a constant power density.

Figs 7 and 8 compare laser micro-milling results at 3.8-µJ pulse energy for pulse durations of 2.9 ns and 20 ns, respectively. Clearly, laser micro-milling achieves a better surface quality at shorter pulse duration at the expense of a worse material removal efficiency for a given pulse energy. We observed the same trend at 2.9-µJ and 1.9-µJ pulse energies. In order to quantify the surface quality, a 3D mapping was achieved on a portion of the bottom of the trenches using an interferometric sensor (PhotoMap 3D from Fogale Nanotech). The roughness average of the surface (S_a) was calculated from the data. The results shown in Fig. 6(b) confirm what has been observed from the SEM images, i.e., the surface quality expressed in roughness deteriorates with increasing duration of the pulses. Therefore, the best surface quality and the maximum efficiency are not obtained with the same pulse duration. Trade-offs in the laser process have to be considered (and the versatility of our laser platform allows for it) with respect to the relative importance given to efficiency and roughness.

This behavior can however be overcome by the ability of the MOPA laser to rapidly switch between two pulse shapes. Most of the laser milling can be accomplished using the pulse duration that results in the best material removal efficiency, and completed with a few layers ablated using the pulse duration that results in a smoother surface. This is illustrated in Fig. 9, where 20 layers of material were removed using the same operating conditions as shown in Fig. 8 followed by 4 layers using the operating conditions giving the best surface finish as shown in Fig. 7. This two-step process can be implemented in real time. Compared to laser polishing,[12] this approach offers the additional advantage of completing the laser micro-milling process with pulses of shorter duration resulting in a decreased HAZ. Consequently, the integrity of the grain microstructure of the material is better preserved,[13] since layers of the thermally modified material of the large HAZ created at longer pulse durations are removed by this two-step process. Nevertheless, the flexibility of INO MOPA fiber laser allows also for the implementation of proper conditions for laser polishing (pulse durations up to 80 ns) in cases where deemed appropriate.

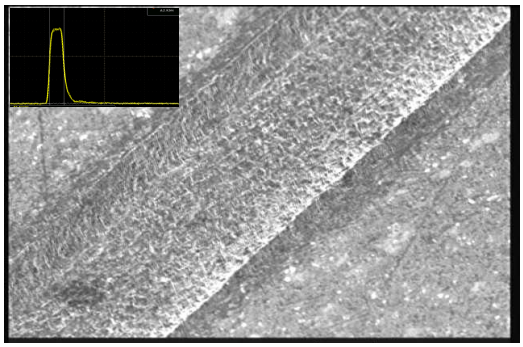

Fig. 7. Energy = 3.8 µJ, Efficiency = 2.76 µm^3/µJ
Power Density = 1219 MW/cm^2, Δt = 2.9 ns.

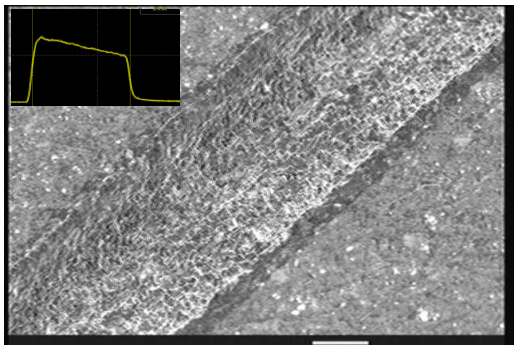

Fig. 8. Energy = 3.8 µJ, Efficiency = 7.89 µm^3/µJ
Power Density ~ 188 MW/cm^2, Δt = 20 ns.

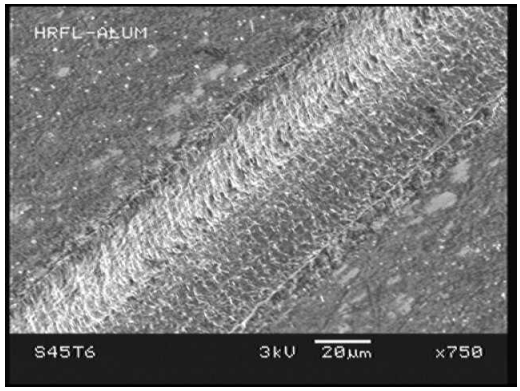

Fig. 9. Micro-milling using the parameters as described in Fig. 8 (20 layers) followed by micro-milling using the parameters as described in Fig. 7 (4 layers). Energy = 3.8 µJ, Overall efficiency = 6.91 µm^3/µJ.

Fig. 10 shows the influence of two-power pulse shapes on the laser micro-milling efficiency and on the surface roughness for 30-ns pulses of a given laser pulse energy. Compared to the square-shaped pulse (shape D), shape E gives the best results in terms of material removal efficiency for pulse energies of 2.9 µJ and 3.8 µJ. The influence of the pulse

shape is even more striking near the material removal threshold, since no material removal occurs at 1.9 µJ, except for shape F. The effect can partly be explained by the different peak power densities reached within the pulse. But, this is not the only factor since the curves in Fig. 10(a) would then exhibit symmetry similar to the pulse shape symmetry along the x-axis. Another part of the explanation is related to the high thermal conductivity of aluminum. The time needed to reach the vaporization temperature is given by $t_v = (\pi/4)K\rho c((T_v - T_0)/[(1-R)I])^2$, where K, ρ and c, respectively, are the thermal conductivity (2.1 W/cm·K for Al), density (2.7 g/cm^3 for Al), and heat capacity (0.9 J/g·K for Al) of the material, T_v is the vaporization temperature (2740 K for Al), T_0 is the ambient temperature (298 K), R is the surface reflectivity (≈ 0.5 at 1064 nm for Al, strongly dependent on the surface roughness) and I is the power density.[11] For I =122 MW/cm^2, which is representative of the 7.5-ns long "back of the chair" of shape B at 1.9 µJ, t_v ≈ 7 ns. Consequently, the material barely reaches the vaporization temperature, leaving little time for material removal. On the other hand, for shape F at 1.9 µJ, T_0 is now given, for I = 39 MW/cm^2 and t = 22.5 ns (corresponding to the end of the "seat of the chair shape"), by $2(1-R)I\sqrt{t/\pi K\rho c} + 298\,\mathrm{K} \approx 1759\,\mathrm{K}$.[11] This gives a value of $t_v \approx 1$ ns at the peak power density I =122 MW/cm^2 of shape F. Consequently, more than 6 ns are left for the material to vaporize after reaching T_v and significant material removal occurs.

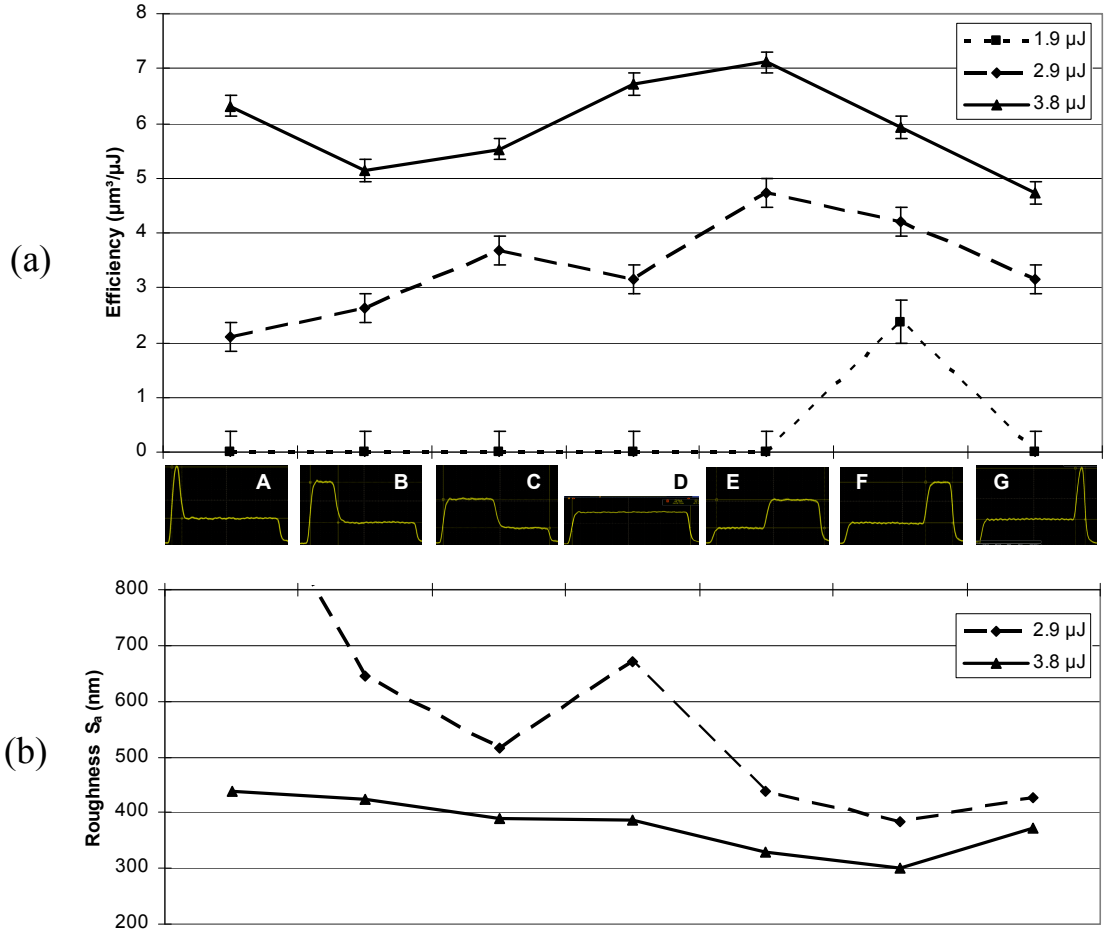

Fig. 10. (a) Material removal efficiency and (b) average roughness in aluminum as a function of pulse shape for pulse durations of 30 ns. The x-axis shows pulse shapes as seen on an oscilloscope.

The same calculation done with power densities corresponding to an energy of 2.9 µJ shows that the time left for material removal with shape F is 1.7 times longer than with shape B, and the same factor is found for the efficiency. Even if this calculation is an approximation, since aluminum properties vary with temperature and surface reflectivity is very dependent on surface quality, it still shows that the preheating conditions and the rise time play a non-negligible

role for laser material removal in high-thermal conductivity metals. Similar analyses can be made for all other pulse shapes for the different pulse energies.

Figs 11 and 12 illustrate laser micro-milling results with 30-ns 2.9-µJ pulses of two different shapes. The peak power densities are close to the vaporization threshold and, clearly, the temporal pulse shape has high influence on both efficiency and surface roughness. In the present case, shape E gives the best results, other shapes, like A or D, creating rough surfaces exhibiting "frozen reflow" of the melted layer.

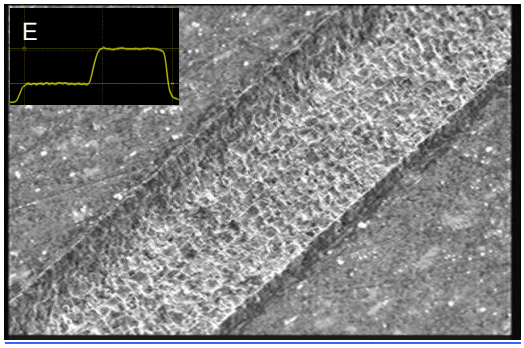

Fig. 11. Energy = 2.9 µJ, Efficiency = 4.74 $\mu m^3/\mu J$
Power Densities = 46-137 MW/cm^2, Δt = 30 ns.

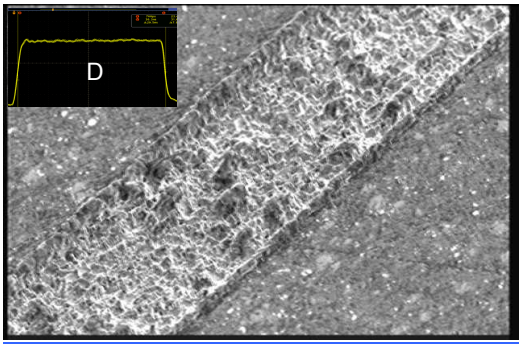

Fig. 12. Energy = 2.9 µJ, Efficiency = 3.16 $\mu m^3/\mu J$
Power Density = 91 MW/cm^2, Δt = 30 ns.

Unlike the results presented in Fig. 6 where the optimum for the material efficiency and for the surface roughness do not occur for the same pulse duration, we observe in Fig. 10 a good correlation between these two aspects as a function of the pulse shape. For example, not only shape E achieves better material removal efficiency than the square-shaped pulse (shape D), it also produces a better surface finish as indicated by the low surface roughness. We thus conclude that the versatility of the MOPA platform to generate all kind of pulse shapes allows for minimizing the trade-off between laser-milling efficiency and laser-milled surface quality.

3.2 Laser micro-milling of stainless steel

Fig. 13 shows the effect of the duration of 4.4-µJ square-shaped pulses on the material removal efficiency ($\mu m^3/\mu J$) of 304 stainless steel. The laser micro-milling at lower pulse energies did not result in significant trench depths. The same analysis as conducted for Fig. 6 applies, except for the fact that the efficiency does not decrease with 30-ns pulses. One will notice that the sloped-top square-shaped pulses give a slightly better efficiency than flat-top square-shaped pulses. Once again, and similarly to the case of aluminum, it was not possible to identify which of the rise time or the slightly different shape was the main factor in explaining the efficiency improvement.

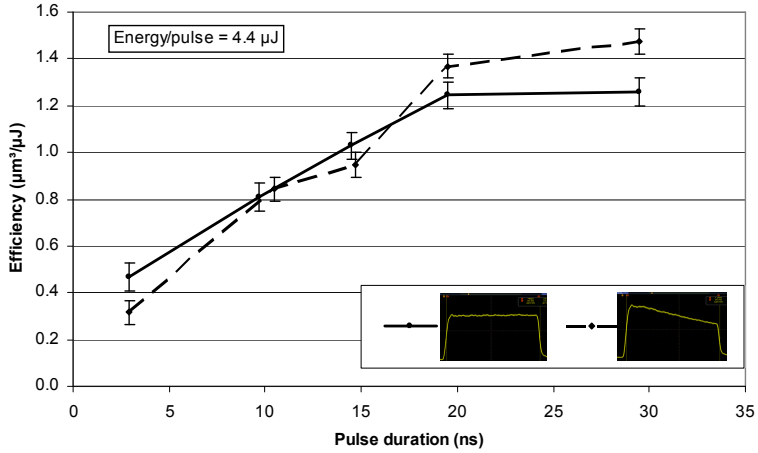

Fig. 13. Material removal efficiency in stainless steel as a function of pulse duration of a square-shaped pulse (flat top and sloped top).

One will also notice a huge difference in material removal efficiency between aluminum (Fig. 6) and stainless steel (Fig. 13). For pulse durations of a few tens of nanoseconds, where the effect of energy lost through thermal diffusion outside the irradiated spot is very limited, the main factor explaining the difference between the two metals is the latent heat of vaporization. An estimate of the material removal efficiency (in absence of plasma effects, thermal diffusion, and changes in reflectivity) is given by $(1-R)/\left[\rho\left(L_v + L_f + c\left[T_v - T_0\right]\right)\right]$.[11] For aluminum, L_v = 1052 J/g, L_f = 395 J/g [11], so that the material removal efficiency can reach approximately 100(1- R) μm^3/μJ. For stainless steel, typical values of the same properties are more difficult to find in the literature. T_v is in the range of 3293 K, ρ =7.7 g/cm^3 and c =0.45 J/g·K. [14] Taking the values of L_v =7106 J/g, L_f =274 J/g for iron [11] as an approximation, we find that the material removal efficiency can reach approximately 15(1- R) μm^3/μJ for stainless steel. Those values give a ratio of approximately 6 between the efficiencies of both materials, which is consistent with the data reported in Figs 6 and 13.

Fig. 14 shows the influence of two-power pulse shapes on the laser micro-milling efficiency and on the surface roughness for a given pulse duration (30 ns) and a given laser pulse energy (4.4 μJ). Compared to aluminum (Fig. 10), the curve in Fig. 14 is symmetric with respect to the square-shaped pulse (shape D) in terms of efficiency, the latter being the most efficient. The peak power density seems to be of importance in stainless steel, along with the fact that thermal diffusion is much smaller compared to aluminum. With K = 0.16 W/cm·K and $R \approx 0.5$, the time t_v to reach the vaporization temperature is less than 1 ns for I =140 MW/cm^2 (peak power density of the 30-ns 4.4-μJ square-shaped pulses) in stainless steel. The material thus reaches the vaporization temperature almost instantaneously on the scale of pulse durations, which is not the case for aluminum. Unlike aluminum, no obvious correlation exists between the material removal efficiency and the surface roughness (Fig. 14 (b)) for the stainless steel. However, one can observe that laser micro-milling started with "the back of the chair" results in a better surface roughness than when the "chair" is inversed.

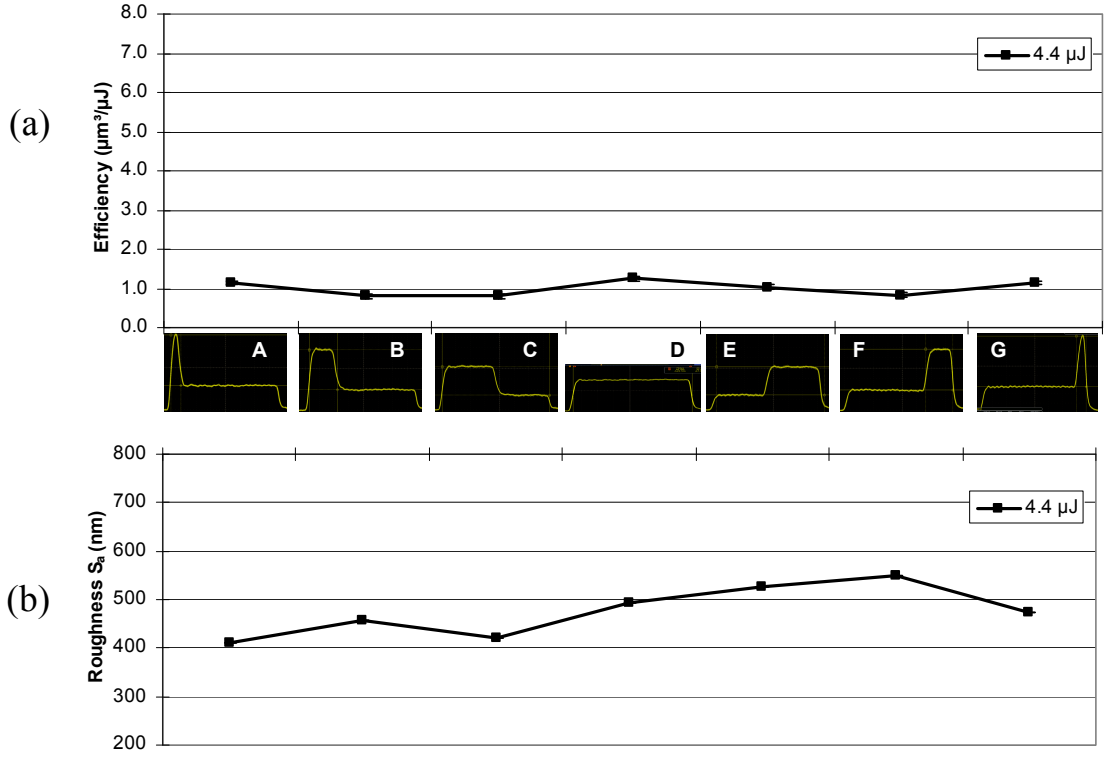

Fig. 14. (a) Material removal efficiency and (b) average roughness in stainless steel as a function of pulse shape for pulse durations of 30 ns. The x-axis shows pulse shapes as seen on an oscilloscope.

The difference in roughness is hardly observable on the SEM images. Indeed, comparing the laser micro-milling results shown in Figs 15 and 16, which illustrate the best and worst cases in terms of roughness, there is little information to differentiate the two laser processes in terms of surface quality. Even less difference exists for the intermediate cases. Also, compared to laser milling in aluminum (Figs 8 and 11), we easily observe the imprint of each individual pulse at the bottom surface of the laser micro-milled channels. Such an effect can also be observed in aluminum, but at a lesser extent and for the shortest pulses only (see Fig 7). Since the characteristic length of thermal diffusion is given by $D = \sqrt{4kt}$, k being the thermal diffusivity (0.85 cm^2/s for aluminum [11] and 0.04 cm^2/s for stainless steel [15]), then for a pulse duration of 30 ns, D = 3.2 µm for aluminum and 0.7 µm for stainless steel. At t = 2.5 ns, D = 0.92 µm for aluminum and 0.2 µm for stainless steel. Across the laser beam diameter (~11 µm) and the distance between two pulses (5-6 µm), the length of thermal diffusion in stainless steel, even for the longest pulses, is negligible. Consequently, there is almost no molten layer in stainless steel that can either be expelled by vapour pressure, or be subject to a reflow process that would blur the imprint of individual pulses. The same is valid in aluminum only at the shortest pulse duration (2.5 ns). Again, the agility of our pulse-shaping fiber laser can circumvent the trade-off between efficiency and roughness by using a two-step process in real time. For example, the process could be to remove layers of material with pulse shape D until the desired depth is reached and finish with a few layers using pulse shape A.

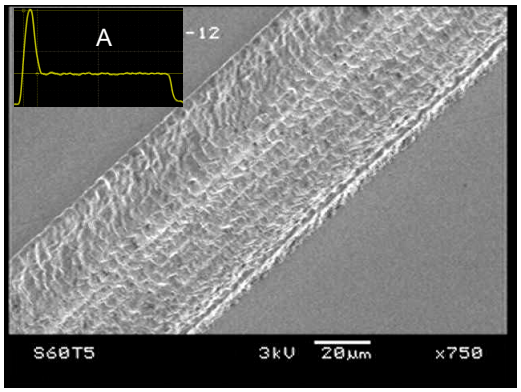

Fig. 15. Energy = 4.4 µJ, Efficiency = 1.14 $\mu m^3/\mu J$
Power Densities = 365-115 MW/cm^2, Δt = 30 ns.

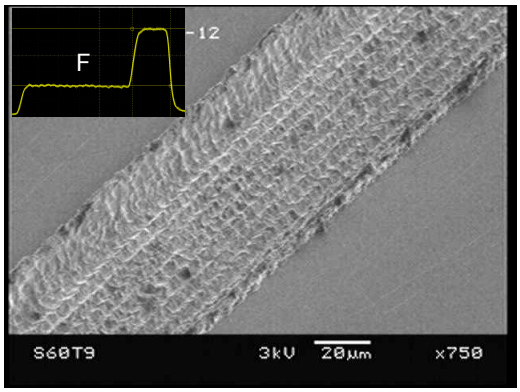

Fig. 16. Energy = 4.4 µJ, Efficiency = 0.83 $\mu m^3/\mu J$
Power Densities = 90-281 MW/cm^2, Δt = 30 ns.

3.3 Laser micro-milling using femtosecond pulses

For comparison, we conducted tests on laser milling aluminum with a femtosecond laser. Most parameters were adjusted to those used with the pulse-shaping laser fiber, such as repetition rate (400 Hz), energy (a few µJ), spot diameter (11 µm), scanning speed (2 mm/s) and groove separation (6 µm). On the other hand, the wavelength of the femtosecond laser is 803 nm (instead of 1064 nm) and should help to remove more material since the absorption coefficient is about three times higher. The main difference is, of course, the pulse duration which is 10^5 times shorter in the case of the femtosecond laser. Fig. 17 shows the laser micro-milling efficiency and throughput as well as the surface roughness as a function of the pulse energy for 200-fs and 20-ns pulses. We recall that the throughput of the laser process, which represents the time to remove a certain volume of material, is related to the material removal efficiency by

$$Throughput = \frac{V_p}{T} = Efficiency \times Incident\ Power \quad \left[\mu m^3/s\right]. \tag{3}$$

In the case of femtosecond pulses, we observed that the efficiency decreases with the pulse energy. This trend can be partly explained by the fact that, even at the lowest energy, the power density was two times higher than the air breakdown threshold. At higher energies, the plasma shielding becomes more important preventing the laser energy to be absorbed efficiently by the workpiece. The energy could be further lowered to obtain better efficiency but it would have been at the expense of the throughput (as shown in Fig. 17(a)). As for the nanosecond regime, the throughput increases with the efficiency for this set of parameters and moreover, for pulse energies higher than 3 µJ, our pulse-shaping laser platform gives better performances than the femtosecond laser. However, laser milling using femtosecond pulses results in a better surface roughness than nanosecond pulses (see Fig. 17(b)). Once again, the flexibility of our laser platform allows someone to quickly select the appropriate pulse shape or duration to improve the surface

roughness. For example, a few additional laser-milled layers using 3-ns pulses improve the surface roughness to a level equivalent to that obtained with femtosecond pulses.

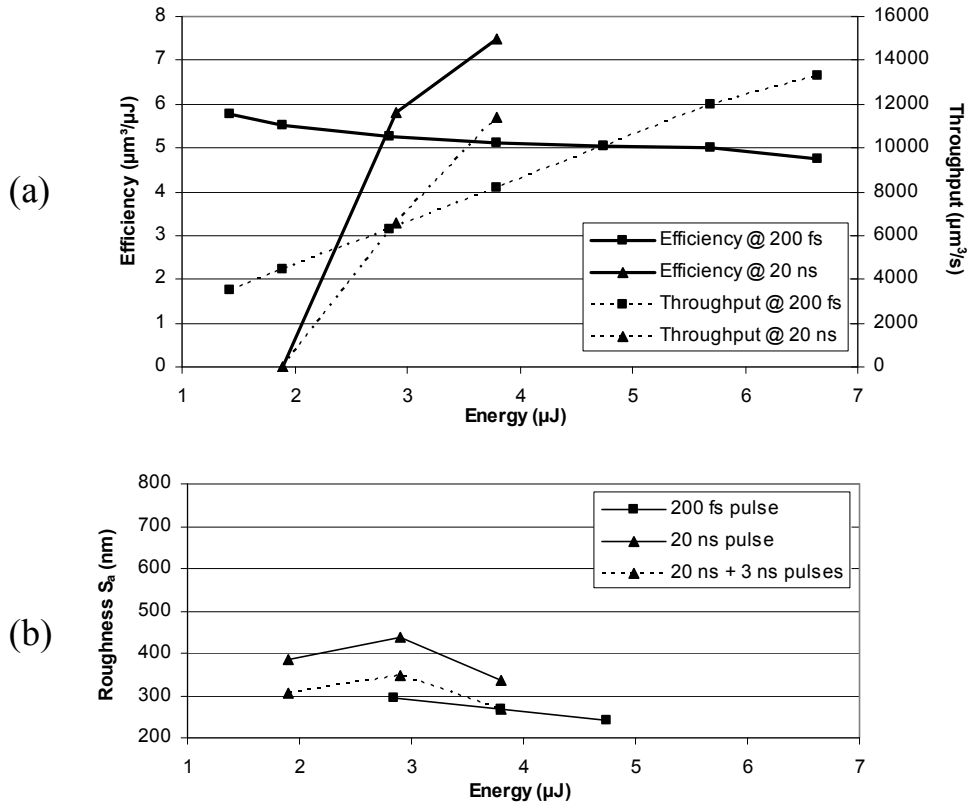

Fig. 17. (a) Material removal efficiency and throughput, and (b) average roughness in aluminum as a function of pulse energy. Comparison between femtosecond and nanosecond pulse durations.

4. CONCLUSIONS

The different results obtained in the micro-milling experiments carried out in this work demonstrate the usefulness of agile pulsed laser sources providing straightforward control over the pulse characteristics (temporal shape, duration, pulse-on-demand capability) in the nanosecond regime. Our results show that the pulse shaping can be advantageously used to develop laser micro-milling processes offering the best conditions for the process throughput or for the surface quality, as both aspects were found to be sensitive to the pulse shape. Moreover, we demonstrated that laser processes including two steps employing different pulse characteristics can be readily implemented for optimizing without trade-off the material removal rate and the surface roughness at the same time. We also showed that such a two-step process developed with our laser source outperforms under similar milling conditions what could be achieved with a femtosecond laser. Furthermore, the cost for the latter is much higher than for a nanosecond-pulse fiber laser offering equivalent pulse energies and repetition rates. For stainless steel, the benefits of the pulse shapes studied in this work were found to be more marginal regarding the surface quality. The lower thermal conductivity of stainless steel compared to aluminum might be responsible for this result. However, our laser system allowed us to maximize the material removal efficiency through the control of the duration of square-shaped pulses. As demonstrated in this preliminary study on laser micro-milling of metals, the pulse shaping agility of our MOPA fiber laser in the nanosecond regime offers at least two major benefits for industrial applications. First, it is the ideal tool to speed up the optimization stage of laser micro-machining processes. Second, its capability to select pulse-to-pulse shapes at high repetition rates allows for the implementation of high-throughput laser processing. Its fine control on energy delivery at the nanosecond scale opens new opportunities for laser-matter interactions research.

REFERENCES

[1] Wang, X., Shephard, J.D., Dear, F.C. and Hand, D.P., "Optimized Nanosecond Pulsed Laser Micromachining of Y-TZP Ceramics", J. Am. Ceram. Soc. 91 (2), 391-397 (2008).

[2] Forsman, A.C., Banks, P.S., Perry, M.D., Campbell, E.M., Dodell, A.L. and Armas, M.S., "Double-pulse machining as a technique for the enhancement of material removal rates in laser machining of metals", J. Appl. Phys. 98, 033302 (2005).

[3] Ancona, A., Röser, F., Rademaker, K., Limpert, J., Nolte, S. and Tünnermann, A., "High speed laser drilling of metals using a high repetition rate, high average power ultrafast fiber CPA system", Optics Express 16 (12), 8958-8968 (2008).

[4] Deladurantaye P. et al., "Pulsed laser light source", US Patent application No. 20060159138, July 2006.

[5] Baird, B. W., Peng, X., Ren, W., Hemenway, D. M., Xu, L., Deladurantaye, P. and Taillon, Y., "Tandem photonic amplifier employing a pulsed master oscillator fiber power amplifier with programmable temporal pulse shape capability" Proc. SPIE 6871, 68712A (2008).

[6] Deladurantaye P., Drolet M., Desbiens L., Taillon Y., Labranche B., Roy V. and Laperle P., "140 μJ, narrow linewidth, robustly single-transverse mode nanosecond infrared fiber laser platform with fine pulse tailoring capability", Proc. SPIE on Conference Photonics North 2009, *to be published*.

[7] Laperle, P., Paré, C., Zheng, H. and Croteau, A., "Yb -Doped LMA Triple-Clad Fiber for Power Amplifiers,", Proc. SPIE, 6453, paper 645308-2 (2007).

[8] Croteau, A., Taillon, Y. and Lauzon, J., "Multi-Clad Doped Optical Fiber", US Patent No.7,068,900 B2, 2006.

[9] Kaldos, A., Pieper, H. J., Wolf, E., Krause M., "Laser machining in die making – a modern rapid tooling process", J. Materials Proc. Tech., 1815-1820 (2004).

[10] Campanelli, S. L., Ludovico, A. D., Deramo, C., "Dimensional accuracy optimization of the laser milling process", Proc. Laser Microprocessing Conference, ICALEO 2006, 298-305 (2007).

[11] Ready, J.F., [Guide to Laser Materials Processing], Edited by S.S. Charschan, Laser Institute of America, Orlando, Chapter 5: Absorption of Laser Energy, 73-95 (1993).

[12] Mai, T.A. and Lim, G.C., "Micromelting and its effects on surface topography and properties in laser polishing of stainless steel", J. Laser Applications 16, 221-228 (2004).

[13] Petkov, P.V., Dimov, S.S., Minev, R.M. and Pham, D.T., "Laser milling: pulse duration effects on surface integrity", Proc. IMechE Vol. 222 Part B: J. Engineering Manufacture, 35-45 (2008).

[14] Karnakis, D., Rutterford, G. and Knowles, M.R.H., "High power DPSS laser micro-machining of stainless steel and silicon for device singulation", Oxford Lasers Limited, Moorbrook Park, Didcot, Oxfordshire, UK (2007).

[15] www.matweb.com/ 304 stainless steel.